A computational study of joint effects of transverse shear and streamwise acceleration on three-dimensional boundary layers

K. Hanjalić, S. Jakirlić and F. Durst
Lehrstuhl für Strömungsmechanik, Friedrich-Alexander Universität, Erlangen, Germany

An initially two-dimensional turbulent boundary layer was subjected simultaneously to a transverse shear, imposed by a moving wall, and a strong streamwise acceleration, and the joint effects were studied computationally by applying a second-moment closure model with new low Re number and wall proximity modifications. The model was previously verified in the computation of several two-dimensional thin shear flows, including the cases in which each of the two considered external effects were present separately. The comparison with the available, though modest, experimental results shows good agreement. The computations show a dominant effect of the imposed transverse shear manifested in a large turbulence production in the initial region of the three-dimensional boundary layer, but the strong acceleration subsequently becomes dominant over the flow and damps the turbulence, leading to eventual relaminarization. The dynamics of the turbulence response, which is strongly dependent on the relation between the magnitudes of the two counteracting effects, was well reproduced by the applied model.

Keywords: turbulent flows; three-dimensional boundary layers; accelerated flows; transverse shear; laminarization; modeling and computations; second-moment closures; low Re number models

Introduction

It is generally believed that any bulk three-dimensionality imposed on initially two-dimensional (2-D) turbulent flows enhances instability and generation of turbulence. Yet in some cases, the experiments as well as direct numerical simulation indicate a reduction of all turbulent stress components. Such are initially 2-D turbulent boundary layers subjected to skewing or otherwise imposed transverse pressure gradients. It was found that all stress components decrease, but the shear stress decreases faster than the normal stresses, leading to a reduction of the turbulence structure parameter, $|\tilde{\tau}|/k$, ($\tilde{\tau}$-shear stress vector in xz-plane) (e.g., Bradshaw and Pontikos 1985, Sendstad and Moin 1991). The effect is opposite if the three-dimensionality is induced by an imposed transverse shear, generated, for example, by a moving wall bounding the flow. Here, the generated turbulence energy is also fed into the spanwise components as compared with only the streamwise component in a 2-D boundary layer. If such a flow is also subjected to a streamwise pressure gradient, as often found in turbomachinery, the combined effects of imposed shear and flow skewing may result in a very different level and structure of turbulence in comparison with a 2-D situation.

A case in point is a shear-driven, three-dimensional (3-D) turbulent boundary layer subjected to a high acceleration. Such flows are encountered in some industrial applications where the flow acceleration is caused by the fluid expansion (as in turbine blade passages) or the negative pressure gradient is intentionally imposed to suppress turbulence and even to promote the flow laminarization. The two externally imposed extra strain rates—the transverse shear (longitudinal vorticity) and the favorable pressure gradient (longitudinal linear straining)—act in an opposing manner. The first enhances turbulence generation in the wall vicinity, whereas the second acts toward damping turbulent fluctuations. Which of these will prevail depends, of course, on their relative intensities. The outcome can be a maintaining turbulent flow or turbulence may die out and the flow will laminarize. Most of the mentioned industrial applications are associated with heat transfer, and its control—enhancement or suppression—can be achieved by optimization of the relation between the imposed shear and acceleration rates.

Another interesting feature of the considered flow, also pertinent to flows in which only one of the considered effects is present, is turbulence dynamics and its response to step changes, as well as to any rapid variation of the mean rate of strain. Different turbulence interactions are known to respond at different rates to the imposition of new conditions. A satisfactory prediction of the variation of turbulence properties on the imposed, new, external effects is a useful test of the modeling hypotheses of various terms in the transport

Prof. Hanjalić and Mr. Jakirlić are currently on leave from the University of Sarajevo, Bosnia, Hercegovina.

Address reprint requests to Professor Hanjalić, Lehrstuhl für Strömungsmechanik, Friedrich-Alexander Universität, Erlangen-Nürnberg Cauerstr. 4, 91058 Erlangen, Germany.

Received 18 August 1993; accepted 20 December 1993

equations, but also a crucial prerequisite for a trustworthy application of the model in complex and nonequilibrium industrial flows.

The separate effects of shear-imposed three-dimensionality and severe acceleration have been investigated in the past. Two-dimensional, accelerating turbulent boundary layers have been studied by Launder (1964), Patel and Head (1968), Jones and Launder (1972) and others. Spalart (1986) performed direct numerical simulation (DNS) of self-similar sink flow boundary layers and produced valuable details of turbulence properties. To the writers' awareness, the only work that considered acceleration in combination with other effects is the recent work of Launder and Loizou (1992), who investigated experimentally the laminarization of 3-D boundary layers in a curved, rectangular-sectioned duct with a progressively decreasing cross-sectional area.

Various types of 3-D turbulent boundary layers have also been reported; a collection of experimental and numerical results can be found in the proceedings by van den Berg et al. (1988). Three-dimensionality created by shear was investigated experimentally by Bissonnette and Mellor (1974), Lohmann (1976) and Fulachier et al. (1982)—all on a cylinder with a stationary front and a rotating aft section. The considered plane, shear-driven, 3-D turbulent boundary layer subjected to acceleration is currently investigated experimentally by Aust et al. (1992) and we have used some of their results for model validation.

The present paper considers a plane, initially 2-D turbulent boundary layer on a flat plate that encounters a transverse motion of the bounding wall, imposing a sudden shear force. Starting from the same or other locations, the flow is also subjected to a severe acceleration created by the opposite wall converging with the bottom plate in the mean flow direction. A schematic of the flow situation considered is given in Figure 1.

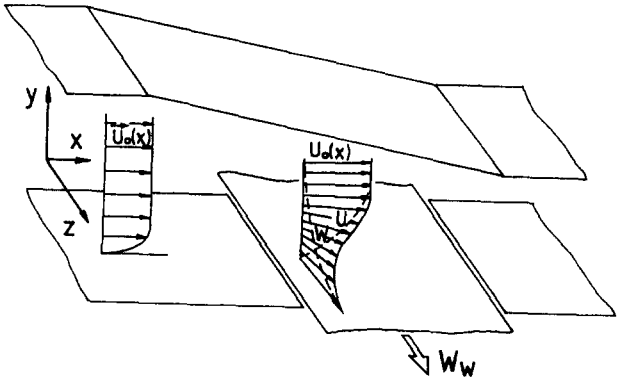

Figure 1 Schematic of the considered flow

The flow has a continuous supply of energy from the moving wall through the work of shear force and, in the absence of other external effects, the eddy structure can be expected to adjust soon to a new, close-to-self-similar situation. A favorable streamwise pressure gradient will impose a continuous stretching of vortex filament in the streamwise direction, causing a gradual but continuous adjustment of turbulence structure and eventual relaminarization if the energy input is insufficient. Such an event may cause drastic consequences (e.g., a sudden decrease of the heat transfer at the bounding wall).

Notation

a	Turbulence structure parameter, $\sqrt{\overline{uv}^2 + \overline{wv}^2}/2k$
a_{ij}	Anisotropy of the turbulent stress tensor, $a_{ij} = \overline{u_i u_j}/k - 2/3\delta_{ij}$
A	Flatness of the stress anisotropy, $A = 1 - 9/8(A_2 - A_3)$
A_2	Stress anisotropy second invariant, $A_2 = a_{ij}a_{ji}$
A_3	Stress anisotropy third invariant, $A_3 = a_{ij}a_{jk}a_{ki}$
C	Empirical coefficient
C_f	Wall friction factor, $C_f = 2\tau_w/Q_e^2$
e_{ij}	Anisotropy of the dissipation rate tensor, $e_{ij} = \varepsilon_{ij}/\varepsilon - 2/3\delta_{ij}$
E	Flatness of the dissipation rate anisotropy, $E = 1 - 9/8(E_2 - E_3)$
E_2	Second invariant of the dissipation rate anisotropy, $E_2 = e_{ij}e_{ji}$
E_3	Third invariant of the dissipation rate anisotropy, $E_3 = e_{ij}e_{jk}e_{ki}$
f	Empirical damping function
H	Boundary-layer shape parameter
Q	Intensity of the mean velocity vector, $Q = \sqrt{U^2 + (W_w - W)^2}$
k	Kinetic energy of turbulence, $k = 0.5(\overline{u^2} + \overline{v^2} + \overline{w^2})$
K	Acceleration parameter for 2-D flows, $K = \nu/U_e^2(dU_e/dx)$
K^*	Acceleration parameter for 3-D flows, $K^* = \nu/Q_e^2(dQ_e/dx)$
n_p	Unit vector normal to the wall, $n_p(0, 1, 0)$
p	Static pressure
P_{ij}	Production of turbulent stresses ($P_k = 0.5P_{ii}$)
Re_t	Turbulence Reynolds number, $\mathrm{Re}_t = k^2/(\nu\varepsilon)$
$U, V, W, (U_i)$	Mean velocity components in x, y and z directions respectively
U_e	Free stream mean velocity
U_τ	Wall friction velocity
W_w	Moving wall velocity
$u, v, w, (u_i)$	Components of velocity fluctuation in x, y and z directions respectively
x, y, z	Streamwise, normal-to-wall and spanwise coordinates
x_R	Referent position along the flow

Greek symbols

β	Angle between the wall shear stress vector and free stream mean velocity
δ	Boundary-layer thickness
Δ	Reference boundary-layer thickness ($\Delta = 0.0254$m)
$\in_{ijk}$	Third-rank unit tensor
ε_{ij}	Stress dissipation rate tensor
ν	Kinematic viscosity
Φ_{ij}	Pressure-strain term in the equation for Reynolds stresses

Subscripts and superscripts

e	Free stream
n	Direction normal to the wall
w	Wall
$\tilde{}$	Root mean square (rms) values
$+$	normalized with inner wall scales (U_τ, ν)

In other cases, the relaminarization in some parts of the flow may be just desirable to prevent negative effects of high turbulence on the quality of an industrial process or product (like in the case of film coating on a solid surface) while still ensuring a sufficient transport of heat and mass at the wall and in the adjacent thin fluid layer. Defining a suitable criterion for the onset of laminarization is, therefore, of significant theoretical and industrial relevance.

For 2-D accelerating boundary layers, the most common criterion for laminarization is the acceleration parameter $K = \nu/U_e^2(dU_e/dx)$ (see Notations). Alternatively, the non-dimensional pressure gradient $p^+ = -\nu/(\rho U_\tau^3)(dp/dx)$ can be used. The critical value of K at which a turbulent boundary layer reverts to laminar was experimentally found to be between 2.8 and 3.2 $\times 10^{-6}$. The DNS of Spalart (1986) gave a more precise specification of the critical K, which seems to be closer to the lower experimental limit. The corresponding range of critical p^+ is between 0.021 and 0.024.

These criteria lose their meaning in a shear-driven 3-D flow, since the enhancement of the turbulence level due to the transverse wall movement, which delays the reverse transition, depends strongly on the wall velocity W_w. In fact, it is expected that the critical value of K will increase with an increase in W_w. Perhaps the more appropriate criterion is $\Delta_\tau^+ = \nu/(\rho U_\tau^3)d\tau/dy$ suggested by Patel and Head (1968), but this parameter is impractical because it employs the local gradient of the total shear stress. Alternatively, the transverse wall movement can also be accounted for by replacing the streamwise velocity U_e in K by the vector sum of the free stream and wall velocity (i.e., $K^* = \nu/Q_e^2(dQ_e/dx)$ where $Q_e = \sqrt{U_e^2 + W_w^2}$. At a high acceleration, K^* will gradually approach the value of K in an analogous 2-D flow, since the effect of W_w will gradually fade with a rapid increase in U_e along the flow. Although numerical modeling may, in principle, be employed to establish a form of characteristic laminarization criterion for any geometry, we have restricted ourselves, at present, to the computation of the flow considered at specific conditions defined by the prescribed K and W_w. The aim of the work was to test and to demonstrate the predictive ability of the same turbulence model (which proved successful in predicting several simpler 2-D and 3-D flows) in a new situation, in which two or more extra strains are present simultaneously. Of particular relevance to the geometry considered here are the model verifications in 2-D, strongly accelerating boundary layers and in constant pressure, shear-driven 3-D turbulent boundary layers, which, as will be shown later, showed a very good agreement with the available experiments. One may argue that an extrapolation of a turbulence model to a new situation, in which the model was not tested before, may not lead to trustworthy conclusions. Indeed, because of the nonlinear character of stress-strain interactions, even a successful verification of the model in situations where various extra strain rates are isolated gives no guarantee that the model will perform well if different effects are present simultaneously. Yet, a trustworthy extrapolation to an unknown situation, in which various effects may appear in different combinations, is the major prerequisite to turbulence models, if they are expected to serve as predictive tools.

The results presented here may serve as a proof—though only partial due to limited availability of experimental data—of model applicability to the computations of a flow exposed simultaneously to two types of extra strains, the transverse shear and streamwise strain, even if both extra strain rates are very high.

Governing equations and turbulence model

The considered flow has a character of a 3-D boundary layer that can be described by the mean momentum equation for the streamwise and spanwise coordinate direction (for notation see Figure 1).

$$\rho\left(U\frac{\partial U}{\partial x} + V\frac{\partial U}{\partial y}\right) = -\frac{\partial P}{\partial x} + \frac{\partial}{\partial x}\left(\mu\frac{\partial U}{\partial x} - \rho\overline{u^2}\right) + \frac{\partial}{\partial y}\left(\mu\frac{\partial U}{\partial y} - \rho\overline{uv}\right) \quad (1)$$

$$\rho\left(U\frac{\partial W}{\partial x} + V\frac{\partial W}{\partial y}\right) = \frac{\partial}{\partial x}\left(\mu\frac{\partial W}{\partial x} - \rho\overline{wu}\right) + \frac{\partial}{\partial y}\left(\mu\frac{\partial W}{\partial y} - \rho\overline{wv}\right) \quad (2)$$

Note that there are no changes in the spanwise direction ($\partial/\partial z = 0$), but the changes in the streamwise direction are induced both by the acceleration and by the transverse shear. Also, all three components of the shear stress play an important role. The lateral mean velocity component V was evaluated from the continuity equation.

The closure of the mean momentum equations was achieved by means of a second-moment model that implies the solving of the transport equations for turbulent stresses and for the energy dissipation rate. The presence of extra strain rates generally invalidates the universal law of the wall, so that the use of the conventional wall functions becomes inapplicable. This is particularly the case when a strong acceleration is imposed that progressively thickens the viscous sublayer and may lead to laminarization. For such cases, but also for most other complex turbulent flows, the essential feature of a reliable model is its ability to account for the low Re number and wall proximity effects in a general manner, which will allow the integration of the governing equations up to the wall, irrespective of its shape, with the use of exact wall boundary conditions. For that reason, we consider the turbulence transport equations in a general form as follows:

$$\frac{D\overline{u_iu_j}}{Dt} = \frac{\partial}{\partial x_k}\left[\left(\nu + C_s\frac{k}{\varepsilon}\overline{u_ku_l}\right)\frac{\partial\overline{u_iu_j}}{\partial x_l}\right] - \left(\overline{u_iu_k}\frac{\partial U_j}{\partial x_k} + \overline{u_ju_k}\frac{\partial U_i}{\partial x_k}\right) + \Phi_{ij} - \varepsilon_{ij} \quad (3)$$

$$\frac{D\varepsilon}{Dt} = \frac{\partial}{\partial x_k}\left[\left(\nu + C_\varepsilon\frac{k}{\varepsilon}\overline{u_ku_l}\right)\frac{\partial\varepsilon}{\partial x_l}\right] - C_{\varepsilon_1}\frac{\varepsilon}{k}\overline{u_iu_j}\frac{\partial U_i}{\partial x_j} - C_{\varepsilon_2}f_\varepsilon\frac{\varepsilon\tilde{\varepsilon}}{k} + C_{\varepsilon_3}\nu\frac{k}{\varepsilon}\overline{u_ju_k}\frac{\partial^2U_i}{\partial x_j\partial x_l}\cdot\frac{\partial^2U_i}{\partial x_k\partial x_l} + C_{\varepsilon_4}f_4k\frac{\partial U_i}{\partial x_j}\frac{\partial U_l}{\partial x_m}\in_{ijk}\in_{lmk} \quad (4)$$

For the dissipation equation, we have adopted the form (equation 4) of Hanjalić and Launder (1976), which already contains all necessary modifications and has been verified in several types of flows within the framework of second-moment closures. Equation 4 was extended by the addition of the term suggested by Hanjalić and Launder (1980), the last term in Equation 4, which enhances the effect of irrotational strain. In the considered flow, $\partial U_i/\partial z = 0$, so that the term can be reduced, for convenience, to the same form as in 2-D flows, $C_{\varepsilon_4}(\overline{v^2} - \overline{u^2})(\partial U/\partial x)\varepsilon/k$, which now separates the contribution of the shear strain from the irrotational one.* This term, found also to improve predictions of flows with strong adverse pressure gradients, proved beneficial in computing the sink flows at higher K and in predicting laminarization at appropriate conditions.

*The application of this term in the original invariant form, as given in Equation 4, in low Re number flow regions, requires a damping function f_4 in order to satisfy the conditions very close to the wall. With the modified form, as used here, there is no need to introduce f_4.

The recent appearance of direct numerical simulation (e.g., Kim et al. 1987) showed that Equation 4 does not reproduce a proper behavior of ε very close to the wall. However, since ε is of no practical relevance per se, except to serve for computing of the turbulence scale and of the components of stress-dissipation ε_{ij}, this defect is usually compensated by adequate modeling of the other terms in the $\overline{u_i u_j}$ equation, above all of Φ_{ij}, ε_{ij} and, to some extent, of turbulent transport. The modeling of these terms is still the major task in designing general, second-moment closure models. Over the past few years, the search for adequate models of the pressure-strain and dissipation terms has been intensified and a number of new proposals (in conjunction with both the high and low Re number models) have been recently published. The flow considered in the present paper is geometrically simple and one may be tempted to apply the most complex forms of models available in literature that are tailored to satisfy exactly the important mathematical constraints and are expected to mimic physics more appropriately than the simpler models. However, the complex models are still insufficiently tested and often pose numerical difficulties when applied to geometrically more complex flows. In view of possible application of the model considered here to more general 3-D cases, we have adopted an approach that is based on relatively simple but widely verified standard high-Re-number, second-moment closure and concentrated on modifications of the models of Φ_{ij} and ε_{ij}, which would allow both the integration up to the wall in various types of wall flows and adequately account for low Re number effects on the bulk flow. The rationale of the adopted models of the major terms in Equations 3 and 4 is briefly outlined.

The modeling of the turbulent transport has been usually regarded as relatively unimportant in simple equilibrium wall flows, where its role is overshadowed by the source terms. Besides, the simple gradient form usually gives a right qualitative representation. In 3-D flows, this may not be true, since the turbulent transport has no preferential direction and cross-diffusion terms become important, so that the use of a general coordinate-frame-invariant form is more appropriate. Yet, Schwarz and Bradshaw (1993) recently showed that the noninvariant "generalized" gradient expression performed in a pressure-skewed 3-D boundary layer on the flat floor of a duct with a 30° bend almost equally erratic as the more elaborate and tensorially invariant models, reproducing some components remarkably well and some erroneously. However, as in 2-D wall flows, the participation of the turbulent transport terms in the total stress budget remains relatively small even in the 3-D boundary layer considered. Anticipating that the same conclusion applies in the flows considered here, we adopted this simple model, as written in Equations 3 and 4.

For the pressure strain terms, we adopted also the simplest linear models for both the slow and rapid parts, $\Phi_{ij,1}$ and $\Phi_{ij,2}$. To be fully consistent with this approach, we have also retained the standard wall reflection terms $\Phi^w_{ij,1}$ *and* $\Phi^w_{ij,2}$ of Gibson and Launder (1978). A justification for this may be found in the report of Schwarz and Bradshaw (1993), who tested several linear and nonlinear models of Φ_{ij} in the 3-D boundary layer—though only in the fully turbulent flow outside the viscosity-affected region. They found that most of the tested models performed remarkably well and concluded that in fairly simple 3-D flows, the nonlinear forms have no noticeable advantage.

Viscosity effects and wall damping within the viscous sublayer have been modeled in the past by introducing damping functions in terms of nondimensional wall distance y^+ or $\mathrm{Re}^+ = k^{1/2}y/\nu$, turbulence Re number $\mathrm{Re}_t = k^2/\nu\varepsilon$ and, more recently, the eddy flatness parameter $A = 1 - 9/8(A_2 - A_3)$. The last two parameters are invariant to coordinate transformation and reduce to zero at the wall, also satisfying thus far the turbulence two-component limit. Besides, A approaches the value of 1 if the turbulence approaches the isotropic conditions, so this parameter can be conveniently employed to model the effects of turbulence anisotropy on various interactions. Among a number of modifications proposed over the past few years, the models of Launder and Shima (1989) and Launder and Tselepidakis (1993) seem to be the most general, since they employ only the invariant variables to define the damping functions. The first model contains a great degree of empiricism implemented in several functions that were tuned to satisfy a broader range of boundary layer flows. Shima (1991) reported a reasonable overall agreement with experiments and DNS results for several types of boundary-layer flows with basically the same linear model for Φ_{ij}, though in some cases slight readjustments of the coefficient were necessary. However, apparently his model produced laminarization of a sink flow at a much smaller K than the commonly adopted critical value. Launder and Tselepidakis substantiate the arguments for various modeling details by more exact reasoning, albeit recognizing severe limitations of the conventional one-point closure approach, which came to the surface especially in the near-wall region. They performed a fine tuning of their nonlinear model in the plane channel flow at two Re numbers to reproduce turbulent stresses in very good agreement with DNS data, though the stress balances still departed considerably. They did not report on the performance of the model in other situations, but the high numerical sensitivity of the model (discussed in a private communication) gives not much prospect for its wider application in more complex flows.

The present model is an outcome of our endeavor to arrive at a model that should satisfy basic physical constraints, even though this may be achieved by introducing empirical functions. However, we insisted on the approach in which the necessary modifications are achieved in terms of invariant turbulence parameters. This option, as compared with more general ones in which the satisfaction of various mathematical constraints is achieved by the forms of modeled expressions themselves, without additional empirical functions, seems to give a higher degree of sturdiness, which should make the application of the model in more complex turbulent flows easier. This argument may sound unconvincing, but one should recall that most general models have been derived merely by imposing kinematic (tensorial properties) constraints without much concern over the actual physics that the terms represent. With the adopted linear models for the parts of the pressure-strain term, we follow to some extent the approach taken by Launder and Shima (1989) insofar as to define the coefficients in Φ_{ij} in terms of Re_t and A with several small novelties, which were partly necessitated by our form of ε equation, differing substantially from the equation of Launder and Shima. A major novelty is the inclusion of the flatness parameter of the dissipative eddies E defined in analogy with the flatness of the stress anisotropy A. These modifications, together with those in the expression for the dissipation rate tensor ε_{ij} ensured that all terms in the modeled equation satisfy the asymptotic and limiting turbulence states in the case of infinite and vanishing Re_t or close to a solid wall where the turbulence approaches a two-component limit. The adopted forms of the model of the pressure-strain terms are summarized as

$$\Phi_{ij,1} = -C_1 \varepsilon a_{ij} \tag{5}$$

$$\Phi_{ij,2} = -C_2(P_{ij} - \tfrac{2}{3}P_k\delta_{ij}) \tag{6}$$

$$\Phi^w_{ij,1} = C^w_1 \frac{\varepsilon}{k}(\overline{u_k u_m}n_k n_m \delta_{ij} - \tfrac{3}{2}\overline{u_i u_k}n_k n_j - \tfrac{3}{2}\overline{u_k u_j}n_k n_i) f_w \tag{7}$$

$$\Phi^w_{ij,2} = C^w_2(\Phi_{km,2}n_k n_m \delta_{ij} - \tfrac{3}{2}\Phi_{ik,2}n_k n_j - \tfrac{3}{2}\Phi_{kj,2}n_k n_i) f_w \tag{8}$$

where the coefficients have been defined as

$$C_1 = C + A^{1/2}E^2,\ C = 2.5AF^{1/4}f,\ F = \min(A_2\ 0.6)$$

$$f = \min\left[\left(\frac{\mathrm{Re}_t}{150}\right)^2, 1\right]$$

$$C_2 = 0.75A^{1/2};\ C_1^w = 1 - 0.7C;\ C_2^w = \min(A, 0.3)$$

$$f_w = \min\left[\frac{k^{3/2}}{2.5\varepsilon x_n}, 1.0\right]$$

and

$$A = 1 - \tfrac{9}{8}(A_2 - A_3) \quad A_2 = a_{ij}a_{ji} \quad A_3 = a_{ij}a_{jk}a_{ki}$$

$$a_{ij} = \frac{\overline{u_iu_j}}{k} - \frac{2}{3}\delta_{ij}$$

$$E = 1 - \tfrac{9}{8}(E_2 - E_3) \quad E_2 = e_{ij}e_{ji} \quad E_3 = e_{ij}e_{jk}e_{ki}$$

$$e_{ij} = \frac{\varepsilon_{ij}}{\varepsilon} - \frac{2}{3}\delta_{ij}$$

The dissipation rate tensor ε_{ij} was expressed in the form proposed by Hanjalić and Jakirlić (1993).

$$\varepsilon_{ij} = f_s\varepsilon_{ij}^* + (1 - f_s)\tfrac{2}{3}\delta_{ij}\varepsilon \tag{9}$$

$$\varepsilon_{ij}^* = \frac{\varepsilon}{k}\frac{[\overline{u_iu_j} + (\overline{u_iu_k}n_jn_k + \overline{u_ju_k}n_in_k + \overline{u_ku_l}n_kn_in_j)f_d]}{\left(1 + \frac{3}{2}\frac{\overline{u_pu_q}}{k}n_pn_qf_d\right)} \tag{10}$$

where

$$f_s = 1 - \sqrt{A}E^2 \qquad f_d = (1 + 0.1\mathrm{Re}_t)^{-1} \qquad n_p(0, 1, 0)$$

The model employs the Re number function f_d to damp the wall correction and prevents its prolonged effect outside the viscous region. The new function f_s is expressed in terms of the flatness parameter of the dissipative scales E. The use of E to define the switch over from the isotropic to nonisotropic dissipation (when the wall approaches) was inspired by the DNS data, which indicate a much higher degree of anisotropy in ε_{ij} in a plane channel—at least at the two considered Re numbers, 5600 and 14000—than hitherto anticipated. In fact, DNS data show that the anisotropic form $\varepsilon_{ij} = \varepsilon\overline{u_iu_j}/k$ is a good approximation for all three normal components up to $y^+ \approx 60$. This behavior cannot be simulated either in terms of Re_t or A. For the considered bulk Re numbers, Re_t departs already at $y^+ = 10$, whereas A remains more or less uninfluenced by the bulk Re number and would produce a similar degree of anisotropy even at very high Re numbers, where the dissipation anisotropy remains confined to the narrow, near-wall region. The parameter E seems to respond adequately to the bulk Re number influence.

The coefficients in the ε equation take the following values: $C_\varepsilon = 0.18$, $C_{\varepsilon 1} = 1.44$, $C_{\varepsilon 2} = 1.92$, $C_{\varepsilon 3} = 0.35$, and $C_{\varepsilon 4} = 3.0$. The last two coefficients have been slightly modified in comparison with the originally proposed values in conjunction with the applied model of the stress equation, after the testing was performed over a broad range of test cases, to achieve the best overall agreement in a number of low Re number flows. The only empirical function in the ε equation is $f_\varepsilon = 1 - (C_{\varepsilon 2} - 1.4)/C_{\varepsilon 2}\{\exp[-(\mathrm{Re}_t/6)^2]\}$, introduced by Hanjalić and Launder (1976) to ensure a switch from the initial to the final period of decay of isotropic turbulence at the appropriate turbulence Re number.

Numerical method

Computations were performed by a finite-volume Navier-Stokes numerical solver for 2-D flows in an orthogonal coordinate system with collocated variable arrangement. The code was modified by selective interpolation of the transport equations for the turbulent stresses instead of interpolating stresses themselves at the control cell boundaries, which improved the convergence. For the flows considered here, the code was parabolized in so far that the pressure gradient was specified explicitly and the V component of the mean velocity calculated from the continuity equation. Apart from these approximations, the method retains all the features of a general code and accounts for the streamwise gradients of all variables. Some preliminary tests performed by applying the full (elliptic) form of the equations gave almost identical results for the 2-D boundary layer and sink flows, apart from the initial adjustment region of the solution domain. The typical number of grid points across the flow was about 100, clustered in the region close to the wall so that at least 80 points were placed within the boundary layer and, of these, at least 30 were within the viscosity-affected zone. The nearest point close to the wall was typically at $y^+ \approx 0.1 - 0.2$. The solutions were obtained by marching downstream and solving the equations at each streamwise position by the iterative lower-upper (ILU) method after Stone. A typical size of the forward step was 2–5 percent of the boundary layer thickness.

Results and discussion

The applied model was tested in a range of thin shear flows at low and high Re numbers, including a plane channel, wall boundary layers at constant and variable pressure, sink flows at several acceleration parameters (including the case with laminarization) and in a 3-D boundary layer on a rotating cylinder. For illustration we shall first present some results for simpler flows in which only one of the considered effects—the acceleration or shear-induced three-dimensionality—were present.

Two-dimensional sink flows

Spalart (1986) provided direct numerical simulation for three values of the acceleration parameter K. We will present here some results only for his highest value, $K = 2.75 \times 10^{-6}$, which is close to the critical one at which the reverse transition occurs. For this value of K, Spalart still obtained a self-similar, fully turbulent solution with a small but persistent turbulence level. Also, some results will be presented for $K = 3.2 \times 10^{-6}$, which has been regarded as sufficiently high to cause flow laminarization irrespective of the initial turbulence level. Figures 2–4 show a comparison between our computations and DNS results for the mean velocity profile and components of turbulent stresses, showing a very good agreement, particularly close to the wall. For the lower values of K, the agreement is

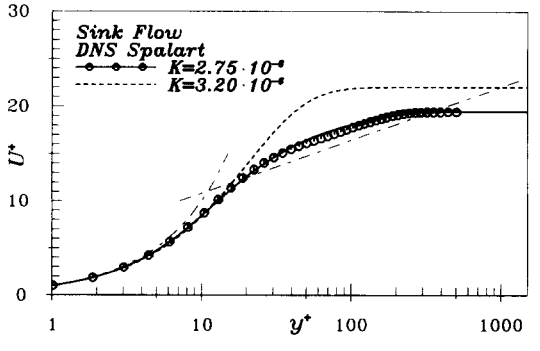

Figure 2 Mean velocity profile in a 2-D sink flow

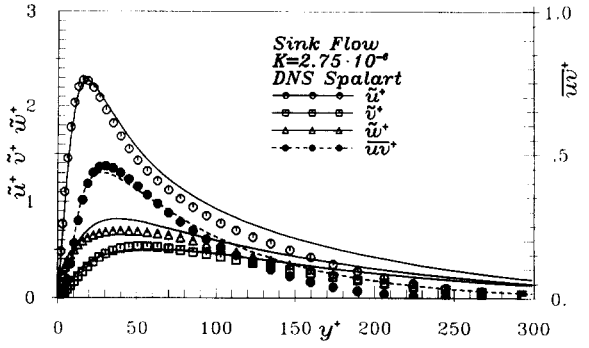

Figure 3 Turbulence intensities and shear stress components in a 2-D sink flow

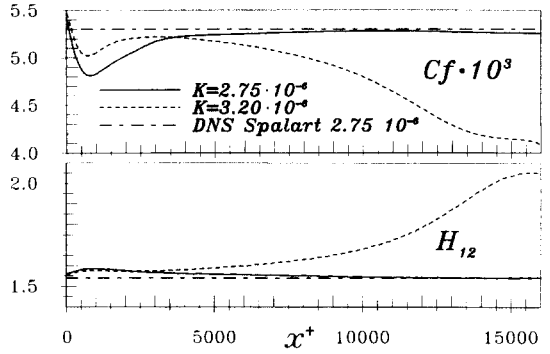

Figure 5 Friction factor and shape parameter in sink flows for two values of K: initial profiles are the same

equally good. As can be seen in Figure 3, the maximum turbulent shear stress is less than half of the wall shear stress and occurs at $y^+ \approx 30$. The shape of the profiles of the normal stresses resembles those in a constant-pressure boundary layer or channel flow at corresponding Reynolds numbers, but with an obvious reduction of all three components, particularly in the outer flow region. It is also noticeable that the damping due to acceleration affects the spanwise component $\tilde{w}^+$ the most and the streamwise component $\tilde{u}^+$ the least, increasing the stress anisotropy in the near-wall region as compared with a constant-pressure boundary layer.

An important test for turbulence models is the ability to predict proper asymptotic behavior of all turbulence properties as the wall is approached. Because the fluctuations normal to the wall die out faster than those in the plane parallel to the wall, the turbulence approaches the two-component limit. Figure 4 shows the log-log plot of all stress components in the near-wall region, with an indication of limiting theoretical slopes. A very good agreement between the DNS results and present computations, achieved in both, the magnitudes and slopes of the predicted stress components, apart from $\tilde{w}^+$, can serve as a proof that the model reproduces the asymptotic, near-wall behavior and satisfies the two-component limit. The disagreement in $\tilde{w}^+$ probably originates from the deficiency of the simple model of the pressure-strain term, but does not much affect the other flow parameters, at least in 2-D situations.

In order to illustrate the model performance in the limit of vanishing Re_t and in predicting the laminarization, we present in Figure 5 the evolution of the friction factor C_f and the shape parameter H along the flow for $K = 2.75 \times 10^{-6}$ and for $K = 3.2 \times 10^{-6}$. Both solutions were obtained by starting from the DNS data for the smaller K. In both cases there is an adjustment length indicating incompatibility of the modeled

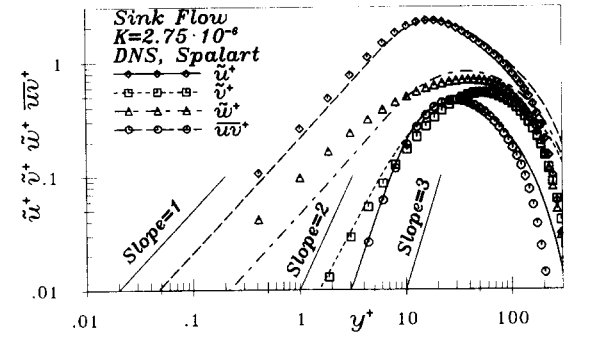

Figure 4 Blowup of turbulence intensities and shear stress in the near-wall region in a 2-D sink flow

equations and initial profiles from the DNS data, especially of dissipation ε. The DNS produced a considerably higher dissipation rate very close to the wall than obtained by the model, so that the turbulent stresses, as well as the wall shear stress, decrease sharply in the initial part of the adjustment length. A full recovery is achieved after the new profiles, which satisfy the modeled equations, are obtained. For $K = 2.75 \times 10^{-6}$, the solution eventually yields the self-similar values very close to the DNS results. Whereas for $K = 3.2 \times 10^{-6}$, the turbulence shows a steady decay and the flow laminarizes as indicated by the typical laminar values of both the friction factor C_f and of the shape parameter H at the end of the solution domain.

Of course, a more severe test of the model would be to check its ability to reproduce the dynamics of the turbulence decay and laminarization for various initial conditions. Unfortunately, this was not possible because of lack of data for comparison. However, a good test of the dynamics of the response of the turbulence model on the external perturbation is an oscillating flow, particularly at a transitional Re number in which forward and reverse laminar-to-turbulent transitions occur within a single cycle, independently of the initial conditions. Such a test, reported by Hanjalić et al. (1993) proved that the same model performed well, reproducing the dynamics of turbulence transition close to a wall in a close agreement with the results of the DNS.

Three-dimensional boundary layer on a rotating cylinder

The next case considered is the initially 2-D turbulent boundary layer along a stationary cylinder that is three-dimensionalized by encountering the rotating cylinder afterbody. We considered, in parallel, two sets of experimental data, those of Bissonnette and Mellor (1974) and of Lohmann (1976). Both experiments are very similar. In Lohmann's flow, the ratio of the transverse wall velocity to the fluid free stream velocity was $W_w/U_e = 1.41$, whereas Bissonnette and Mellor considered two cases, $W_w/U_e = 0.93$ and 1.8, but published the results mainly for the first case, presumably as they were more reliable. Because both sets of data seem to suffer from some inaccuracies, particularly the measurements of turbulent stresses close to the wall, we will present a selected comparison of our computations with results for both flows.

The same cases were reasonably well reproduced by Gibson and Younis (1986) with a high Re number, second-moment closure (though with different coefficients in the model of Φ_{ij}, $C_1 = 3.0$ and $C_2 = 0.3$) and wall functions based on the resultant velocity and wall shear stress vectors. The evidence of the existence of a constant-stress layer close to the wall where

the shear stress and mean velocity vectors are aligned, indicates that a standard, high Re number, second-moment closure gives reasonable predictions of a mildly 3-D boundary layer on a rotating cylinder. Since our interest was primarily in the flows with simultaneously imposed high acceleration, when the wall functions become inapplicable, a verification of our low Re number model in the flow along a rotating cylinder appeared essential for gaining a confidence in the model applicability in a complex flow with simultaneous transverse shear and acceleration.

Figure 6 compares the streamwise and spanwise mean velocity profiles at a number of successive positions along the cylinder with the experimental data of Lohmann (1976). The agreement is generally satisfactory, though for the Lohmann flow our predictions indicate a conspicuous change in the curvature of the U profile at the edge of the inner (spanwise) boundary layer associated with the transverse velocity, which propagates radially outward with the growth of the inner layer along the cylinder and, eventually, disappears. The phenomenon seems to be related to the effect of the transverse shear, which initially tends to reduce the axial velocity close to the wall. It is interesting that the agreement with the data of Bissonnette and Mellor (not shown here) is generally better, possibly because of smaller W_w/U_e, whereas the predictions of transverse velocity are in better agreement with the experiments of Lohmann. The effect of the wall movement on the mean velocity is also reflected in the logarithmic plots (not shown here) of the mean velocity vector, $Q = \sqrt{U^2 + (W_w - W)^2}$ (normalized with the wall shear stress vector), which depart slightly from the experimental results for both cases. It is interesting that Lohmann's data for all stations comply with the standard logarithmic slope, indicating a good validity of the law of the wall, whereas Bissonnette and Mellor's data show a visible departure (though opposite from our predictions), which they attributed to the curvature effects. The latter flow along the 127mm-thick cylinder could be more prone to the curvature effects than Lohmann's flow along the twice thicker cylinder with diameter of 260mm. However, excellent agreements of results of both authors, with the standard logarithmic law for the first measured stations at the stationary cylinders, and inconsistent discrepancies between the two sets of mean velocities along the rotating cylinder, do not support the argument of curvature effects, but rather hint at some inaccuracies in measurements in the near-wall region.

The predictions of the mean flow features are further illustrated in the next two figures. The variations of the total wall friction factors along the flow for the two considered cases (Figure 7) show a sudden rise at the position where the flow encounters the moving cylinder and a subsequent adjustment to an almost constant value corresponding to the self-similar flow on a rotating cylinder. As seen, for Lohmann's case the predicted friction is somewhat higher than the experimental one in the initial region, whereas the agreement for the Bissonnette and Mellor flow is generally satisfactory at all stations. A similar quality of agreement is obtained for the angle between the wall shear stress vector and the free stream velocity, as shown in Figure 8.

The influence of a sudden imposition of the transverse shear on the turbulence structure is illustrated in the next set of figures. The evolution of normal stresses (Figure 9) is reproduced very well at all stations and for both sets of data, as illustrated by the profiles of the root mean square (rms) of velocity fluctuations $\tilde{u}$, $\tilde{v}$ and $\tilde{w}$ (here only Lohmann's flow is shown). The agreement is very good at most stations, though unsatisfactory at some. It should be noted that the agreements and disagreements are not consistent for the two sets of experimental data, indicating possible defects in the hot-wire measurements at some stations in both experiments, especially close to the wall. The model reproduced well the increase in the spanwise normal stress components $\overline{w^2}$, which exceeds the other two in the near-wall region as a consequence of a large energy input due to the transverse shear.

Good agreement has been obtained also for the $\overline{uv}$ shear stress components for both sets of data (also shown in Figure 9) as well as for $\overline{wv}$ for the Bissonnette and Mellor flow (not shown), in spite of the fact that these measurements are prone to inaccuracies when measured with a slanted, hot wire at a

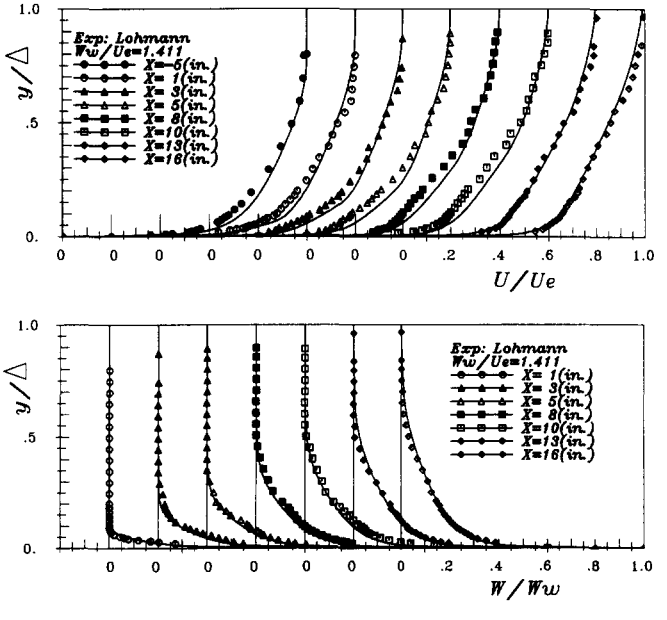

Figure 6 Axial and transverse mean velocity profiles along the flow on a rotating cylinder at constant pressure

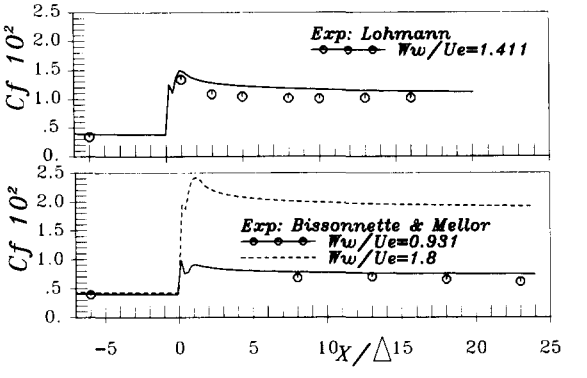

Figure 7 Friction factors along the flows on rotating cylinders

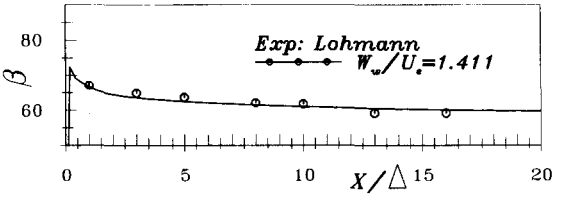

Figure 8 Variation of the angle between the wall shear stress vector and free stream velocity

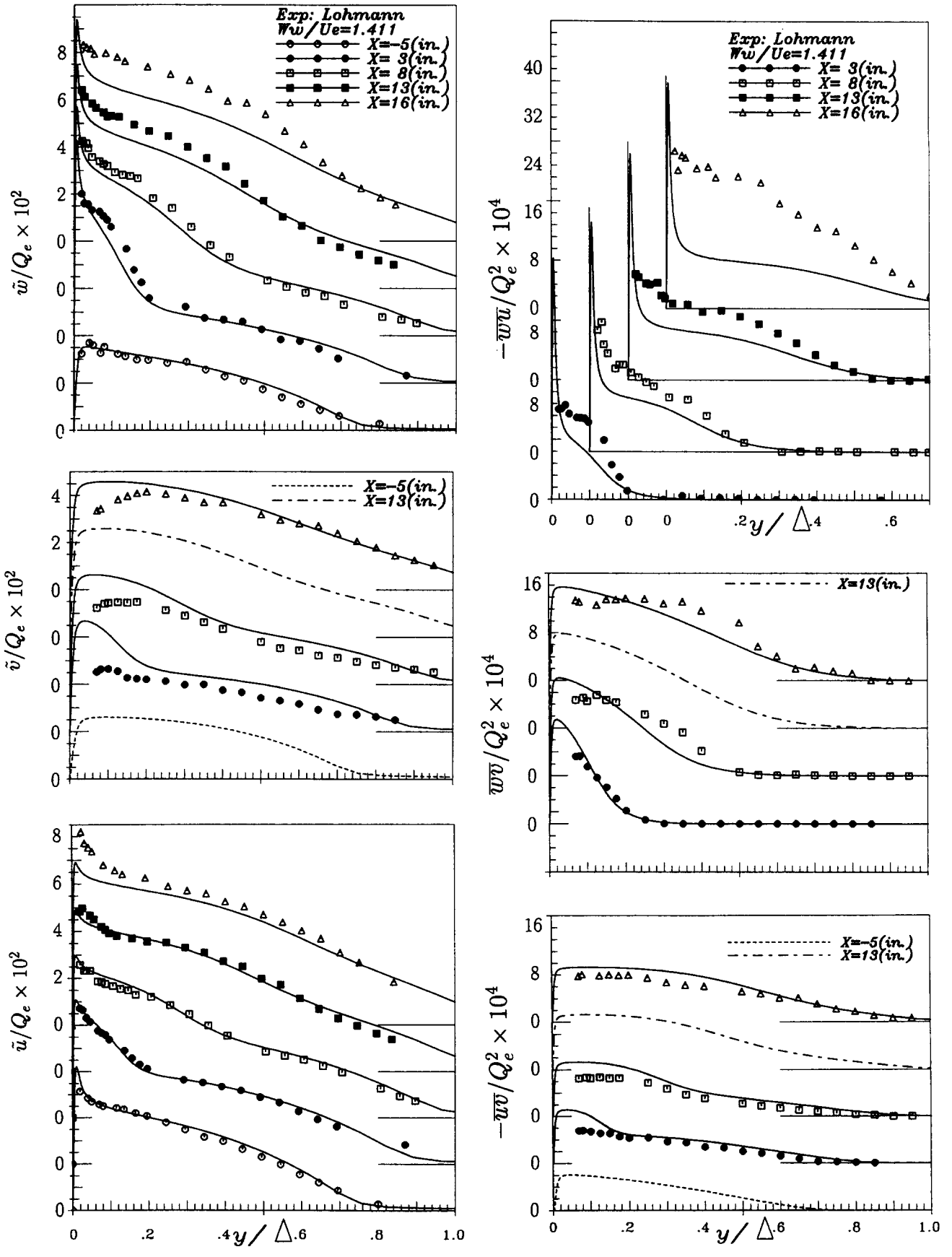

Figure 9 Turbulence intensity and shear stress components along the flows on a rotating cylinder ($W_w/U_e = 1.41$, Lohmann flow)

45° angle with the wall. In fact, our predictions agree particularly well with the results evaluated from the integration of the momentum equations. However, for Lohmann's flow at stations further downstream, the agreement is not satisfactory. Even worse is the agreement for the $\overline{wu}$ component, particularly for Lohmann's flow. The same quality of predictions was reported by Gibson and Younis (1986), and Higuchi and Rubesin (1979). The experiments show high levels of this shear stress component (higher than the other two), which remains almost constant over a progressively larger portion of the boundary layer thickness as the fluid flows along the moving cylinder. High values of $\overline{wu}$ close to the wall are expected, since this is the only stress component to which production both dominating velocity gradients, $\partial U/\partial y$ and $\partial W/\partial y$ contribute. It is surprising that the high stress level persists at such large distances from the wall. Our computations indeed yielded very high peaks close to the wall, but considerably smaller values away from the wall. The same discrepancies were reported by Gibson and Younis (1986), Higuchi and Rubesin (1979) and Shima (1991), although different models have been employed. Of course, the high Re number models could not reproduce the high peaks close to the wall.

The measurements used here for comparison were performed with single hot wires perpendicular to the flow and large errors are not expected. Since the symptoms are similar in both sets of data, though more pronounced in the Lohmann flow, where the ratio W_w/U_e is higher, it seems that a high intensity of $\overline{wu}$ further downstream is a characteristic feature of the considered flow, which none of the applied models is able to reproduce. The production of $\overline{wv}$, P_{wv}, is dominated by the terms $\overline{v^2}\partial W/\partial y$ and, to some extent, by $\overline{uv}\partial W/\partial x$, which are both accurately predicted as seen from the profiles of $\overline{v^2}$, $\overline{uv}$ and W. Similarly, P_{wu} is dominated by $\overline{uv}\partial W/\partial y$ and $\overline{wv}\partial U/\partial y$, which again are well reproduced. The dissipation components ε_{wu} and ε_{wv} are small at the considered Re numbers. Hence, the main source of deficiency should be sought in inadequacies of the simple model of the pressure-straining process, Φ_{ij}, given by Equations 5–8. The region in question is sufficiently far from the wall that the low Re number and near-wall modifications of coefficients should have no effect. Because the models of $\Phi_{ij,1}$ and of $\Phi_{ij,2}$ (although very simple) are given in invariant form, they should not be dependent on the flow orientation, provided, of course, that the model is sufficiently general. The major deficiency probably lies in the wall echo models, Equations 7 and 8, which should simulate a damping of the stress redistribution process Φ_{ij} due to the pressure reflection from the wall. The model employed yields zero values of Φ_{ij}^w for the $\overline{wu}$ component. Although this shear stress does not involve the fluctuations normal to the wall, it does not seem plausible that it will remain unaffected by the wall pressure reflection. It should be recalled that Equations 7 and 8 were derived for 2-D flows parallel to the wall and they have already been shown to yield erroneous effects in cases in which the dominant flow direction is normal to the wall, as in impinging jets. Because of a strong dependence on the local normal distance from the nearest wall, these expressions are also likely to fail in 3-D situations, even if the major flow direction remains parallel to the wall. No attempt was made to modify these expressions for the three-dimensionality effects because they have been regarded as the weakest part of the pressure-strain model and ought to be replaced by a more general model that should be void of the local wall distance. It should be noted that deficiencies in accurately predicting $\overline{wu}$ do not seem to affect the mean flow properties much nor the intensities of turbulence fluctuations, as shown earlier.

A blowup of all stress components in the wall vicinity is shown in log-log plots in Figure 10. No experimental data so close to the wall are available, but the results show good compliance with the theoretical slopes, indicating that the model satisfies the wall asymptotes.

Figure 11 compares the computed structure parameter $a = \sqrt{\overline{uv}^2 + \overline{wv}^2}/2k$ with the experimental results of Lohmann. The large scatter, particularly at $x/\Delta = 8$, which originated from scatter of measured $\overline{uv}$ and $\overline{wv}$, leaves little opportunity for drawing a plausible conclusion on the evolution of the structure parameter a. The computations produced at all stations more or less constant values, $a \approx 0.15$–0.17, in close agreement with the value found in a 2-D wall boundary layer. Lohmann's results for individual stress components at $x/\Delta = 3$,which seem to be most consistent, yield $a \approx 0.135$ up to $y/\Delta \approx 0.6$, whereas for three other stations a is somewhat higher. The experimental data of Bissonnette and Mellor show similar scatter, particularly in the outer region, whereas in the inner wall zone, the parameter a drops to about 0.11 at the first station $X/\Delta = 4$, but increases systematically as the flow progresses downstream. The computations reproduce the

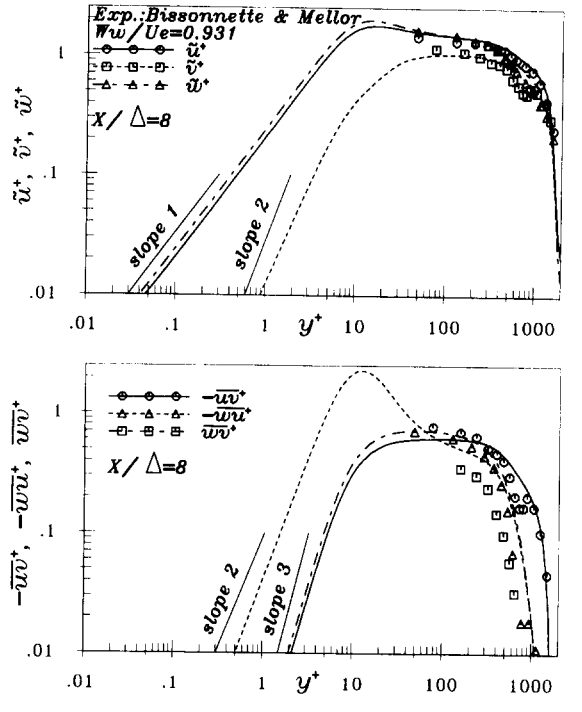

Figure 10 Turbulence intensities and shear stress components close to the wall along the flow on a rotating cylinder ($W_w/U_e = 0.931$, Bissonnette and Mellor flow)

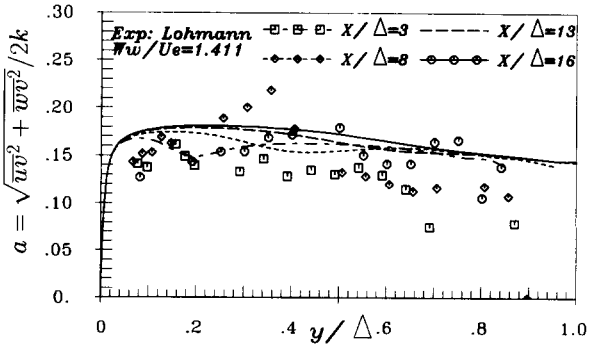

Figure 11 Structure parameter across the flow along a rotating cylinder

trend, but within a much narrower range—from 0.16–0.18. (Bissonnette and Mellor obtained $\overline{uv}$ and $\overline{wv}$ also from the integration of the mean momentum equations. These results give a at all stations between 0.135 and 0.15.) This outcome is in contradiction with the findings in pressure-skewed 3-D boundary layers (Bradshaw and Pontikos 1985, Sendstad and Moin 1991), where a was found to decrease. Indeed, in the present cases the flow is strongly dominated by the imposed shear and conclusions drawn in the pressure-skewed 3-D boundary layer do not seem to be applicable.

An interesting indication of the turbulence response is the evolution of the stress components along the flow. Figure 12 compares the values of normal stresses at three distances from the wall for $W_w/U_e = 1.8$. Following Bissonnette and Mellor, the results were plotted versus the nondimensional axial distance and normalized with the averaged boundary layer thickness $\bar{\delta}$. The agreement can be regarded as satisfactory (still better agreement is achieved by $W_w/U_e = 0.93$), considering that the presented results also involve the estimate of the boundary layer thickness. As mentioned before, the rise of spanwise component follows immediately after encountering the moving wall. Contrary to expectations, two other normal stress components react immediately, in spite of the fact that they receive additional energy not from the mean motion, but from the spanwise component through the pressure redistribution action. A satisfactory reproduction of the response of turbulent stresses on a rapid change of the mean rate of strain is a good indication of the appropriate choice of the time scale in the model of pressure-strain term $\Phi_{ij,2}$ and is of vital importance for the possible extrapolation of the models to predict nonequilibrium and fast-evolving flows.

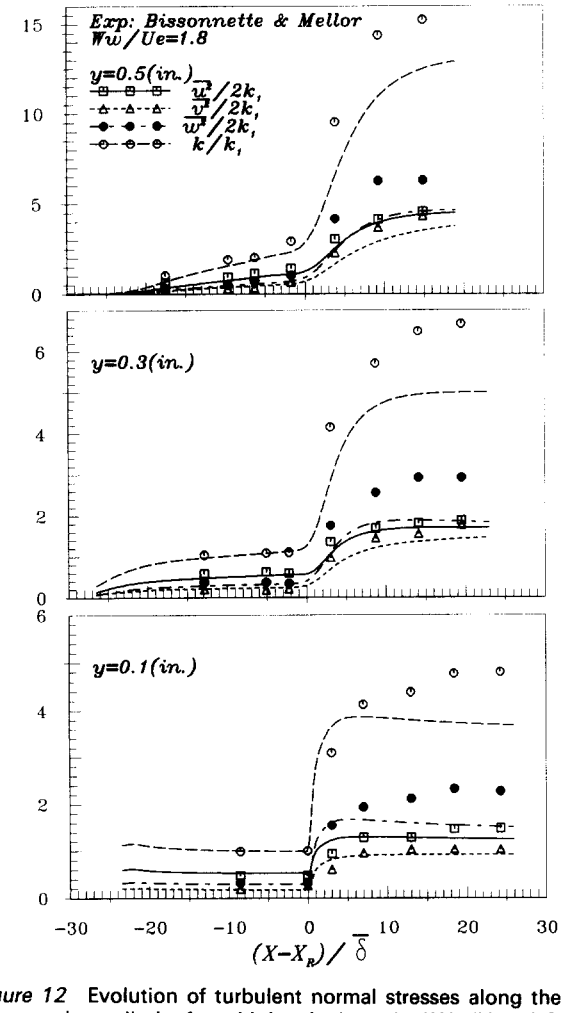

Figure 12 Evolution of turbulent normal stresses along the flow on a rotating cylinder for a high velocity ratio ($W_w/U_e = 1.8$)

Shear-driven, three-dimensional, accelerating boundary layer

We turn now to the flow in which both effects are simultaneously present. Selected was the geometry investigated experimentally by Aust et al. (1992) in which, after 0.5m of a constant-pressure entrance length, a very severe acceleration corresponding to the 2-D acceleration parameter $K = 1.9 \times 10^{-5}$ was imposed, together with a strong transverse strain, with the wall to the initial free stream velocity ratio $W_w/U_{ei} = 3.2$ ($W_w = 2.0$ and $U_{ei} = 0.623$m/s). This ratio decreases progressively as the flow accelerates (Figure 13). The acceleration parameter based on the vector sum of the wall velocity and free stream velocity K^* can be expressed in terms of K for the 2-D flow as

$$K^* = \frac{\nu}{Q_e^2}\frac{dQ_e}{dx} = K \times \left(\frac{U_e}{Q_e}\right)^3 = \frac{K}{\left[1 + \left(\frac{W_w}{U_e}\right)^2\right]^{3/2}} \tag{11}$$

Its initial value is $K^* = 5 \times 10^{-7}$, but it increases progressively and further downstream approaches the 2-D value very fast, as shown in Figure 13.

The only available experimental data are for the streamwise mean velocity and its fluctuations at several locations along the flow. The flow was computed by simulating actual geometry, moving wall velocity and initial free stream velocity. The initial profiles at the onset of transverse shear and acceleration were obtained by letting a thin boundary layer develop 0.5m along the wall at constant pressure, which—apart from the free stream turbulence—was believed to be a close simulation of the experimental setup. In order to maintain turbulence at such a small free stream velocity of 0.623m/s, the thickness of the boundary layer had to be higher than recorded by Aust et al. (1992). Figure 14a shows very good agreement of computed mean velocities with experiments. As the flow accelerates, at first slowly and then more rapidly, the boundary layer becomes thinner with very steep gradients close to the wall, whereas the outer flow retains almost uniform U velocity profiles. A comparison with the 2-D accelerating flow at the same K ($W_w = 0$) indicates a hardly discernible difference in U profiles, particularly further downstream when the ratio W_w/U_e becomes small. However, the acceleration suppresses the growth of the spanwise boundary layer, which remains almost constant at some length and then begins to decrease.

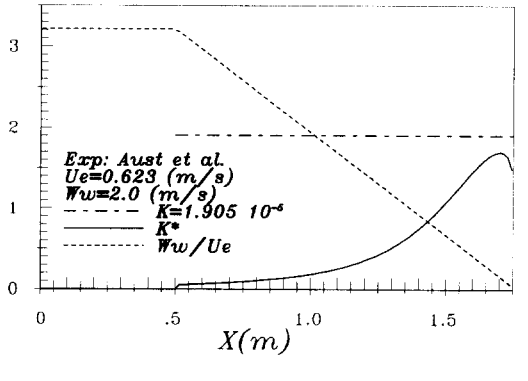

Figure 13 W_w/U_e and K^* variation along the 3-D, shear-driven, accelerating flow

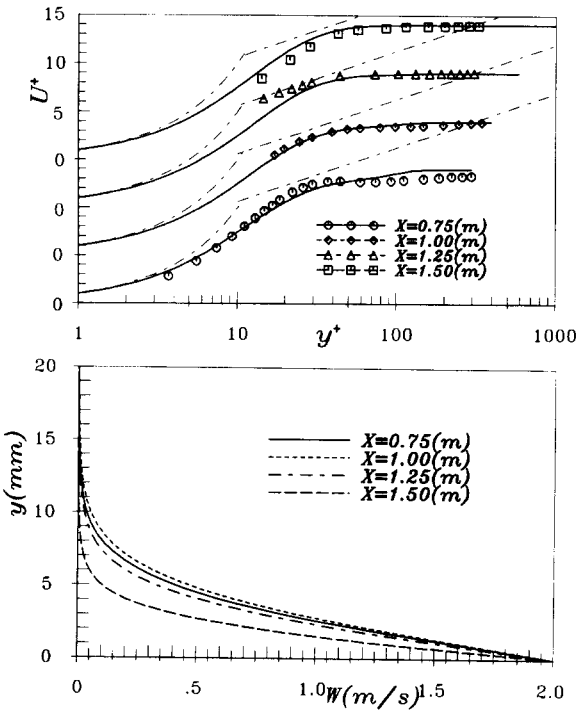

Figure 14 Axial and transverse mean velocity profiles along the 3-D, shear-driven, accelerating flow

This is best seen in the profiles of the spanwise velocity W at the corresponding locations. The initial tendency of increase in W in the outer region of the boundary layer is suppressed as the flow progresses and this trend is soon reversed due to the acceleration. The profiles are distinctly different from those in Figure 6 for constant-pressure flow along a rotating cylinder.

The evolution of the turbulence field is illustrated in Figure 15 where all three components of the velocity fluctuations (rms) and shear stresses are given. Our computations of the streamwise fluctuations did not give satisfactory agreement with measurements of Aust et al. (1992) in the initial portion of the convergent duct. The discrepancies could have been caused by various factors. The experiments were performed by movement of a continuous belt, by which the moving wall was simulated. Slight, but unavoidable bending of the belt, sensitive to the speed and environmental conditions, as well as a bulge at the place where the two ends of the belt were glued, prevented measurements very close to the belt. For these reasons, it was difficult to keep the distance of the measuring points from the belt constant during the experiment and to measure this distance very accurately. Besides, because of the pronounced flow nonequilibrium, the initial turbulence evolution is sensitive to the oncoming turbulence structure. Initial profiles of turbulence level and its scale (initial profiles of ε) were sought by trial and error, but we were not able to reproduce the same initial conditions as measured by Aust et al. However, it appeared that further downstream the initial conditions were not so important because of strong dominance of both extra strain rates. The computations show an almost

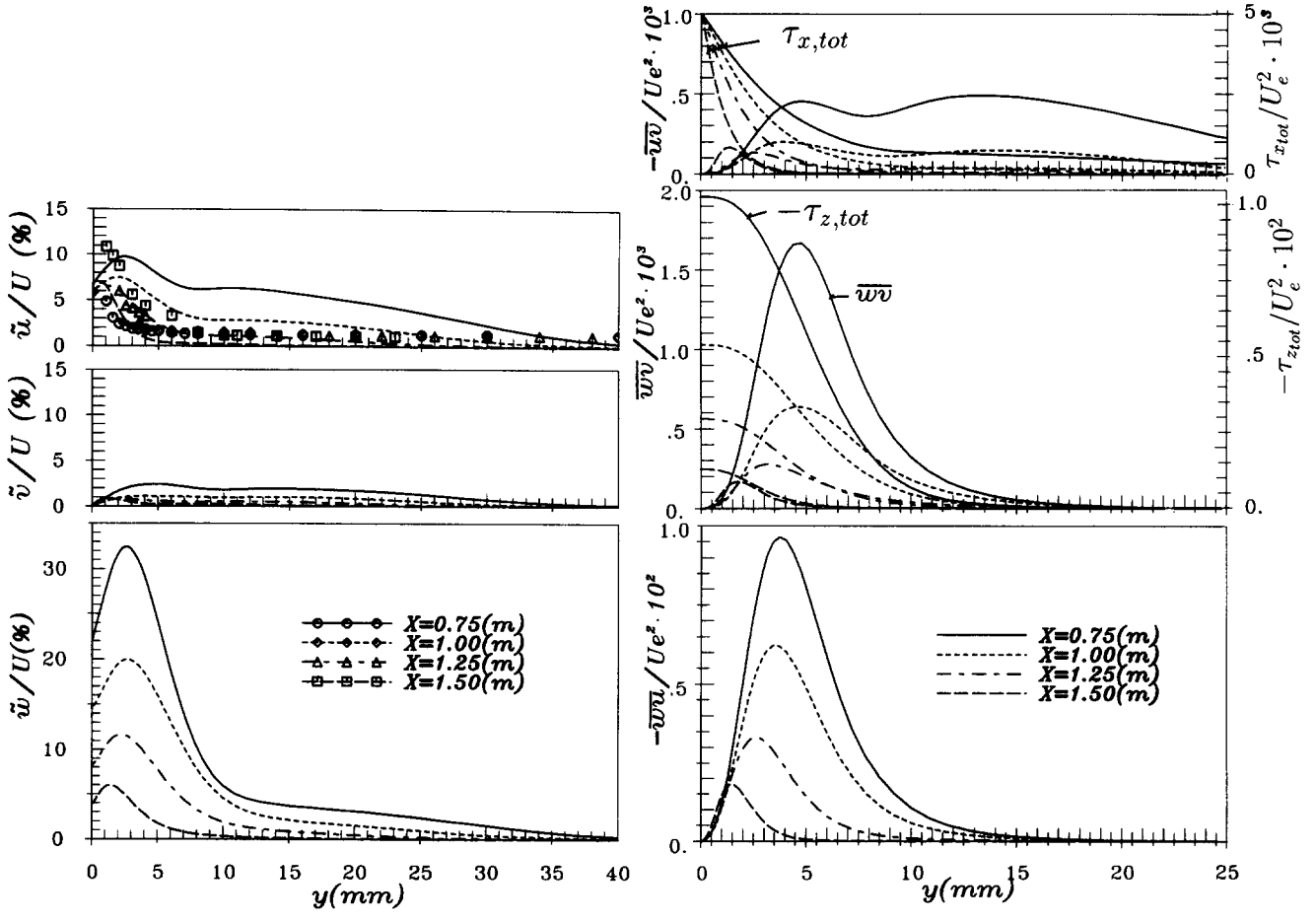

Figure 15 Turbulence intensities and shear stress components in the 3-D, shear-driven, accelerating flow

constant relative turbulence level in the outer region of around 1 percent, but a gradual decrease in peak values close to the wall. The highest damping due to the acceleration is exerted on the $\tilde{v}$ component, which decays fast irrespective of the high shear close to the wall. However, the spanwise component $\tilde{w}$ increases steeply in the initial portion of the flow (note the same scale) due to a high production from the moving wall—preferential feeding due to the transverse shear—but soon begins to decrease as the acceleration effects increase. In fact, in the initial portion of the 3-D flow, the normal stresses tend to follow the pattern found in constant-pressure flow along the rotating cylinder, but preferential damping of the $\tilde{v}$ component due to the acceleration, and a preferential feeding of energy into the $\tilde{w}$ component due to the transverse shear, increase the anisotropy of the turbulent stress field and significantly change the turbulence structure. Further downstream all components decay as the acceleration progressively dominates the transverse shear, but its initial anisotropy pertains for long. The major difference in comparison with a 2-D accelerating boundary layer is that $\tilde{u}$ and $\tilde{v}$ (the latter receiving energy mainly through the pressure-straining action) are affected earlier by the acceleration than the $\tilde{w}$ component, which is directly generated by the transverse shear due to the wall movement.

Shear stress components show a similar behavior. By far the largest increase is in $\overline{wu}$, as expected, whereas $\overline{wv}$ shows only a slight increase, contrary to the flow at constant pressure. In view of the behavior of u and v fluctuations described earlier, which are both suppressed by the acceleration, a strong and steady decay of $\overline{uv}$ is understandable. For comparison, the total shear stress components (viscous plus turbulent) τ_x and τ_z are also given (note different scales) illustrating a rapid diminishing of turbulent contribution along the flow, particularly in the $\overline{uv}$ component.

A preferential damping of v fluctuations and a preferential production of w is best illustrated in Figure 16, where the stress components are presented in the log-log diagram. The theoretical slope of all components is satisfied as in previous cases, but the magnitudes have changed notably. The diagram confirms the often disputed fact that the external effects, if sufficiently strong, penetrate very close to the wall and invalidate the conventional scaling with the inner velocity and length scales U_τ and ν/U_τ, respectively.

Figure 17 shows the structure parameter a, which initially exhibits a visible diminishing in comparison with typical values found earlier in the shear-driven flows at constant pressure, probably because of a higher W_w/U_e ratio. However, as the acceleration progresses, the structure parameter increases and exceeds the value typical for 2-D constant-pressure boundary layers, indicating a faster decay of the turbulence energy than of the shear stress in the plane parallel to the wall.

An illustrative resume of the dynamics of turbulence response is given in Figure 18, which shows the evolution of the maximum values of all stress components along the flow. All components containing the w fluctuations show a sudden jump on encountering the moving wall, particularly $\overline{w^2}$ and $\overline{wu}$, because of a direct effect of production due to spanwise shear, whereas other stress components show a strong decay immediately after the imposition of the flow acceleration. However, the $\overline{u^2}$ component continues to receive energy not only by direct production, $-\overline{uv}(\partial U/\partial y)$, but also from $\overline{w^2}$ due to the pressure-redistributing action. After a sharp decrease immediately after the onset of acceleration, the u component remains more or less constant and even begins to increase, to be suppressed at the end when the feeding from the w component through the pressure-strain interaction becomes insufficient and the flow eventually laminarizes. Figure 18 shows that a full disappearance of turbulence occurs at

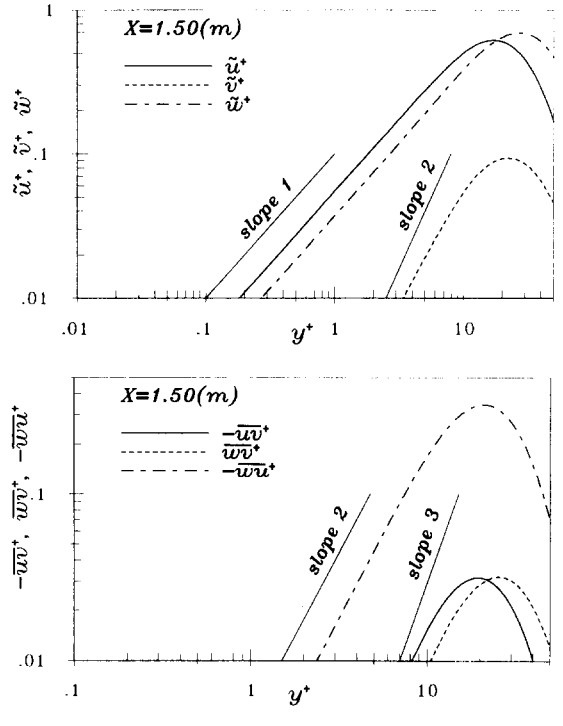

Figure 16 Near-wall behavior of turbulence intensities and shear stress components in the 3-D, shear-driven, accelerating flow

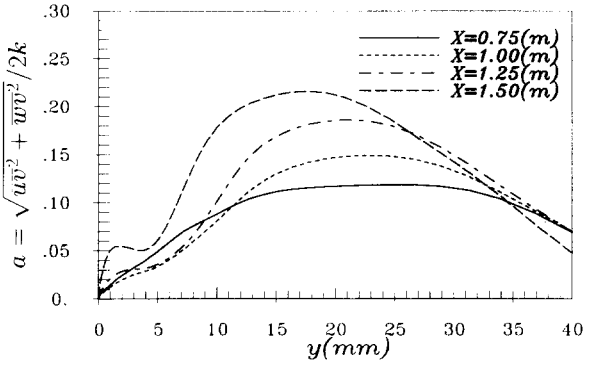

Figure 17 Structure parameter in the 3-D, shear-driven, accelerating flow

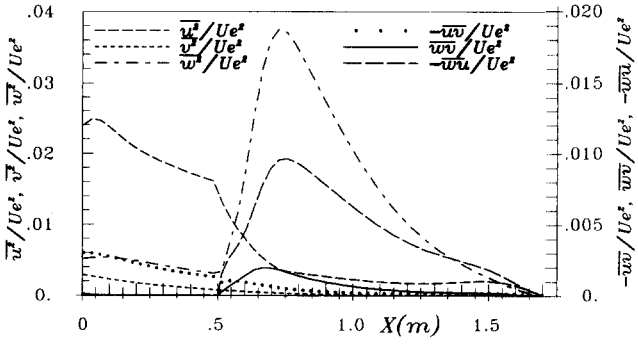

Figure 18 Evolution of maximum turbulent stresses along the 3-D, shear-driven, accelerating flow

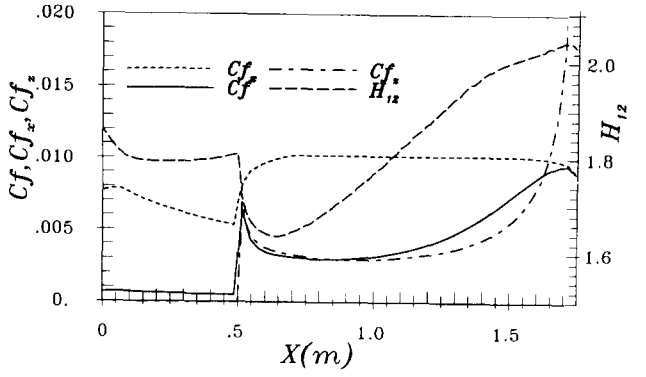

Figure 19 Evolution of friction factors and shape parameter along the 3-D, shear-driven, accelerating flow

$x \approx 1.6$m (i.e., very close to the end of the convergent section of the channel) and at $x = 1.75$m, indicating that $\overline{u^2}$ shows a strong persistence until a very severe acceleration is achieved.

The last figure illustrates the evolution of integral flow parameters along the flow. Figure 19 shows the variation of the total friction factor $C_f = 2\sqrt{\tau_x^2 + \tau_z^2}/(U_e^2 + W_w^2)$, as well as of each component $C_{fx} = 2\tau_x/U_e^2$ and $C_{fz} = 2\tau_z/W_w^2$. All factors increase sharply at the onset of the moving wall. It is interesting to note that C_{fx} retains an almost constant value along the whole flow, which is substantially larger than the initial value in a 2-D turbulent boundary layer prior to transverse shear and acceleration. A similar behavior is exhibited by C_{fz}, which jumps from zero to a peak value when encountering the wall motion, drops slightly and remains almost constant over a large portion of the flow length, but increases sharply at the end of the channel. Since this factor is normalized with W_w, which remains constant, this behavior indicates that τ_z remains constant for a long period and increases steeply only at the end of the convergent channel. The total friction factor also exhibits a sudden increase, but diminishes steadily along the flow, approaching a constant value at the end, which is considerably higher than expected in a laminarized flow. That the flow has eventually become laminarlike, in spite of a substantial turbulence level, is illustrated by the shape parameter H, based on U velocity (Figure 19). Its steady increase up to a value of about 2 is the best indication of the laminarlike form of the mean velocity profile. This seemingly contradictory conclusion that the shape parameter has approached a value typical for laminar flow, while the maximum values of turbulent stresses, as well as the wall friction factor, still indicate a substantial amount of turbulence, can be explained by the fact that the turbulence is concentrated in a relatively thin layer in the buffer zone, which does not affect the mixing in other parts of the flow cross section. An expectation that both parameters H and C_f will behave as in the 2-D accelerating flow, provided K^* becomes large enough (Figure 5), was not justified, since the imposed wall shear delays laminarization irrespective of the value of K.

Conclusions

A modified, second-moment closure model with incorporated low Re number and wall vicinity effects, verified in several simpler flows including 2-D sink flows and constant-pressure, shear-induced, 3-D boundary layers, was used to study the response of an initially 2-D turbulent boundary layer on a flat plate, subjected simultaneously to imposed transverse shear and to a streamwise acceleration. The log-log plots of all stress components in the near-wall region in all three flows considered follow the theoretical slope. For the 2-D sink flows, the computed intensities agreed well with DNS data for all components up to the wall except for a slight discrepancy in $\overline{w^2}$. The predicted behavior can be regarded as proof that the model satisfies the two-component turbulence limit, whereas the predicted laminarization indicates that the model satisfies the limit of vanishing Re_t. The computed streamwise mean velocity profiles at several locations in the 3-D flow with acceleration showed excellent agreement with the available measurements. Although only a partial verification of the predicted turbulence properties was possible because of lack of experimental data, it is believed that the model reproduces well the combined effects of high acceleration and of strong, shear-induced three-dimensionality.

These two opposing external effects exhibit directionally preferential influence on the turbulent stress field. The damping effect due to the acceleration is felt most in the $\overline{v^2}$ component (and, consequently, on shear stresses $\overline{uv}$ and $\overline{wv}$), whereas the transverse shear—and the consequent longitudinal vorticity—enhances the production of the spanwise velocity fluctuations $\overline{w^2}$ and the shear stresses $\overline{wu}$ and $\overline{wv}$. These selective effects cause the turbulence structure to alter and impose a relative increase in stress anisotropy in spite of a progressive damping of the turbulence. The net effect in the considered configuration is a persistence of turbulence—although at a low level—until almost the end of the convergent channel, where the acceleration becomes extremely severe. In spite of turbulence persistence, the flow shows obvious signs of a steady tendency toward laminarization, as anticipated for such a high K parameter. This is particularly visible in the behavior of the shape parameter H based on the U component, which shows a steady increase and approaches the laminarlike level long before the turbulence dies out. However, a continuous secondary turbulence production due to the transverse shear maintains the friction factors along the whole considered flow length at a level that is typical for turbulent flows.

This feature is of significant importance for industrial applications and may have important implications on heat and mass transfer. Although the imposed acceleration is very strong and at $x \approx 1.2$m, K^* already exceeds the critical value for 2-D flows of 3.2×10^{-6}, a high turbulence intensity, concentrated in the w component (produced by the moving wall in the front portion of the channel where acceleration is still weak and the normal gradient of W is very strong), is being convected fast downstream and, in spite of damping, retains a substantial level, also maintaining the u component up to the very end of the channel. Hence, a judgment of the turbulence level based on the measurement of u fluctuations may lead to erroneous conclusions.

Although the evolution of the stress field, presented in Figures, may not be fully trustworthy because of a lack of verification with the experiments, a satisfactory prediction of the turbulence response to separate actions of acceleration and transverse shear give reason to believe that the presented results could not be far wrong. The results also indicate that care should be taken to design properly the flow passage with a transverse moving wall if early laminarization is to be achieved. In spite of the failure to reproduce the behavior of $\overline{wu}$ further downstream, the relatively successful predictions of all other stress components in, for example, a constant-pressure, 3-D boundary layer along a rotating cylinder, can be regarded as an argument in favor of the often questioned ability of turbulence models to account for 3-D effects. These predictions fulfill the expectations of model developers that three-dimensionality per se should not invoke severe deviations if the model was derived in a general coordinate-frame-invariant form and provided that the flow structure is reasonably similar

to that in an analogous 2-D situation. Deficiencies, such as the mentioned failure to reproduce the wall echo in impinging flows, originate usually from the noninvariant, direction-dependent parts of the model and will appear under some circumstances irrespective of whether the flow is 2-D or 3-D.

Directional preferences on the stress field of the two imposed extra strain rates, which extend deeply into the viscous wall region, clearly indicate that only turbulence models that solve differential transport equations for each stress component up to the wall can be expected to reproduce the flow physics adequately.

Acknowledgement

The authors wish to acknowledge the valuable support of the Deutsche Forschungsgemeinschaft (to K. H.) and the International Bureau of the Forschungszentrum Jülich (to S. J.) during their work on the problem reported here.

References

Aust, R., Durst, F., Leister, H. J. and Stadler, D. 1992. (unpublished) LSTM, University Erlangen, Germany

Bissonette, L. R. and Mellor, G. L. 1974. Experiments on the behavior of an axisymmetric turbulent boundary layer with a sudden circumferential strain. *J. Fluid Mech.*, **63**, 369

Bradshaw, P. and Pontikos, N. 1985. Measurements in the turbulent boundary layer on an infinite swept wing. *J. Fluid Mech.*, **159**, 105

Fulachier, L., Arzoumanian, E. and Dumas, R. 1982. Effects of a sudden discontinuity of the strain at the wall of a rotating cylinder; close-to-wall region of the boundary layer. *IUTAM Symp.*, H. H. Fernholz and E. Krause (Eds.), Berlin

Gibson, M. M. and Launder, B. E. 1978. Ground effects on pressure fluctuations in the atmospheric boundary layer. *J. Fluid Mech.*, **86**, 491–511

Gibson, M. M. and Younis, B. A. 1986. Calculation of boundary layers with sudden transverse strain. *J. Fluids Engineering*, **108**, 470–475

Hanjalić, K. and Jakirlić, S. 1993. A model of stress dissipation in second-moment closures. *Appl. Scientific Research*, **51**, 513

Hanjalić, K., Jakirlić, S. and Hadžić I. 1993. Computation of oscillating turbulent flows at transitional Re-numbers *9th Symp. Turbulent Shear Flows*, Kyoto

Hanjalić, K. and Launder, B. E. 1976. Contribution towards a Reynolds stress closure for low Reynolds number turbulence. *J. Fluid Mech.*, **74**, 593

Hanjalić, K. and Launder, B. E. 1980. Sensitizing the dissipation equation to irrotational strains. *J. Fluids Eng.*, **102**, 34

Higuchi, H. and Rubesin, M. R. 1979. Behavior of a turbulent boundary layer subjected to sudden transverse strain. *AIAA Journal*, **17**(9), 931

Jones, W. P. and Launder, B. E. 1972. Some properties of sink-flow turbulent boundary layers. *J. Fluid Mech.* **56**, 337

Kim, J., Moin, P. and Moser, R. 1987. Turbulence statistics in fully developed channel flow at low Reynolds number. *J. Fluid Mech.*, **177**, 133

Launder, B. E. 1964. Laminarization of the turbulent boundary layer in a severe acceleration. *ASME J. Appl. Mech.*, **31**, 707

Launder, B. E. and Loizou, P. A. 1992. Laminarization of three-dimensional accelerating boundary layer in a curved rectangular-sectioned duct. *Int. J. Heat and Fluid flow*, **13**(2), 124

Launder, B. E. and Shima, N. 1989 Second-moment closure for the near-wall sublayer: development and application. *AIAA J.*, **27**, (10), 1319

Launder, B. E. and Tselepidakis, D. P. 1993. Contribution to the modelling of near-wall turbulence. In *Turb. Shear Flows 8*, F. Durst et al. (Eds.), Springer, Berlin

Lohmann, R. P. 1976. The response of a developed turbulent boundary layer to local transverse surface motion. *ASME J. of Fluids Engineering*, **98**, 354

Patel, V. C. and Head, M. R. 1968. Reversion of turbulent to laminar flow. *J. Fluid Mech.*, **34**, 371

Schwarz, W. R. and Bradshaw, P. 1994. Term-by-term tests of stress-transport turbulence models in a three-dimensional boundary layer. *Phys. Fluids*, **6**(2), 986–998

Sendstad, O. and Moin, P. 1991. On the mechanics of 3-D turbulent boundary layers. *Proc. 8th Int. Symp. on Turb. Shear Flows*, Techn. University, Munich, Germany, 5.4

Shima, N. 1991. Prediction of three-dimensional turbulent boundary layers using a second moment closure. *Proc. 8th Int. Symp. on Turb. Shear Flows*, Techn. University, Munich, Germany, 8.2

Spalart, P. R. 1986. Numerical study of sink-flow boundary layers. *J. Fluid Mech.*, **172**, 307

van den Berg, B., Humphreys, D. A., Krause, E. and Lindhout, J. P. F. (Eds.) 1988. Three-Dimensional Turbulent Boundary Layers—Calculations and Experiments. Vieweg, Braunschweig/Wiesbaden